COMMUNICATION

Extracting Molecular Responses from Ultrafast Charge Dynamics at Material Interfaces

Chenglai Wang^{†a}, Yingmin Li^{†ξa}, Wei Xiong ^{a,b}

Received 00th January 20xx, Accepted 00th January 20xx

DOI: 10.1039/x0xx00000x

We introduce a new data analysis method, which can be applied to transient vibrational sum-frequency generation spectroscopy to reveal hidden molecular dynamics of charge transfer at molecular heterojunction interfaces. After validating the method, we used it to extract molecular dynamics at organic semiconductor/metal interfaces, which was otherwise dominated by electronic dynamics. Such an ability can advance understanding of the roles of molecules in interfacial charge transfer dynamics.

Charge transfer at interfaces induced by photoexcitation affects the efficiency and performance of molecular optoelectronic materials, quantum heterojunctions, organic flexible electronics, and selectivity and activities of photo-electrical catalysts. ^{1–8} In the charge transfer processes, photons first excite bounded electron-hole pairs, referred to as excitons, in the donor. ^{9,10} The excitons dissociate into electrons and holes by overcoming the Coulomb interaction, so that the electron can transfer to the acceptor side of the interfaces. Both electrons and holes interact with the molecular environment during the charge dynamics. Currently, charge dynamics in inorganic heterojunctions are understood well. ^{11,12}

In contrast, heterojunctions involving organic molecules that are prepared by solution-phase processes (e.g., spin-coating) creates complicated interfaces with various molecular conformations. The dynamics in organic/inorganic heterojunction interface include exciton dynamics, free charge (electrons and holes) carrier dynamics, and molecular dynamics. Here, molecular dynamics represents the transient responses of molecules, due to the interactions between charges and molecules, e.g., the role of molecules in charge

separation, and how excitons or free charge carriers affect molecules. Among all these dynamics, molecular dynamics during charge transfer processes are less studied. An understanding of the interactions of molecular species and excited charges in organic molecular interfaces is needed to design and create higher-performing organic optoelectronics, quantum heterojunctions, and photocatalysts. However, observation of molecule-charge interaction is challenging because not only it happens on ultrafast timescales and requires molecular specific detection, but also the charge transfer interfaces are hidden between bulk phases. This challenge makes probing the interplay between molecules and charges during charge dynamics difficult by surface techniques, such as STM and AFM.

We have recently used transient vibrational sum-frequency generation (VSFG) to follow ultrafast charge dynamics at molecular interfaces, spin-coated Poly(3-hexylthiophene) (P3HT) on gold surfaces. 18,22 In these experiments, a visible or near IR pulse triggered charge transfer, and the VSFG probed the interfaces during charge transfer. VSFG is a second-order nonlinear optical signal similar to second harmonic generation (SHG). VSFG uses an IR pulse to excited specific vibrational modes that are upconverted by a near IR pulse to virtual states, which subsequently emit coherent signals at the sum of the near- and mid-IR frequencies. VSFG, therefore, adopts interface-sensitive from SHG. Different from SHG, VSFG probes electronic transition through the NR background, and molecular species by vibrational modes, like IR spectroscopy. Therefore, transient VSFG can reveal local molecular responses to the ultrafast charge dynamics. 23-25 Using this method, we observed ultrafast dynamics corresponding to charge transfer and recombination.

However, in most transient VSFG experiments, metals often have large nonresonant (NR) contributions to the signal, which dominate the scans. The NR signal is generated by impulsive electronics responses to the laser fields, which reports electronic dynamics at interface.²⁶ As a result, the molecular dynamics were mixed with the NR electronic dynamics. In ref (18), we analyzed the dynamics by

Electronic Supplementary Information (ESI) available: [details of any supplementary information available should be included here]. See DOI: 10.1039/x0xx00000x

Materials Science and Engineering Program, University of California, San Diego, La Jolla, California 92093, United States

^{b.} Department of Chemistry and Biochemistry, University of California, San Diego, La Jolla, California 92093, United States

ζ.Current affiliation: Seagate Technology, San Jose, Cupertino, California, 95014, United States

[†] These authors have equal contributions

COMMUNICATION Journal Name

spectral fitting each molecular vibrational features and the NR signals. This analysis concluded that the face-on molecular conformation could allow direct charge transfer from gold to P3HT. However, such data analysis is tedious. We later added heterodyne detection (HD) to the transient VSFG setup, to resolve the spectral phase²², which enabled molecular responses to be disentangled from nonresonant dynamics.^{27–30} Nonetheless, the molecular responses were still overwhelmed by the NR signals that were at least one order of magnitude larger than the former. Thus, we needed to develop a method to extract time-dependent molecular dynamics from the convoluted transient VSFG measurements.

In this communication, we present a new data analysis method to disentangle resonant molecular and NR electronic dynamics. This method allows us to inspect how specific molecules involved in charge transfer. The key idea relies on that the phase of NR spectra is constant, whereas the phase of molecular resonances is frequency-dependent.^{29,31,32} For example, a VSFG signal can be written as

$$S_{HD-VSFG} \propto A_{NR} * e^{i\varphi} + \sum A_R * \frac{1}{(\omega - \omega_R) + i\Gamma}$$
 eq.1

Where A_{NR} , and φ are the amplitude and phase of the nonresonant signal, A_R , ω_R , and Γ are the amplitude, resonant frequency, and linewidth of various molecular resonances. The resonant features could be molecular vibrational and electronic transitions, and both

the resonant and nonresonant features implicitly include the interfacial electric induced signal as $\chi^{(3)} E_{\text{interface}}^{33-38}$, where $\chi^{(3)}$ is the third-order nonlinear susceptibility, and $E_{\text{interface}}$ is the electric field at interfaces. By multiplying equation 1 with $e^{-i\varphi}$, it can make the NR only exist in the real part, and make the imaginary part be purely composed of the phase-rotated molecular resonances (the second term in eq. 1). We can then apply a few data processing procedures to fully separate and retrieve the molecular spectra, as shown below.

To examine this method, we first built a model data and used it as the ground truth to test the method. The model data was composed of two molecular resonant signals, one NR background, which decay (see Fig.2 for details of each component) in the ways described by equation 2

$$R(\omega, t) = [L_1(\omega) + NR(\omega)] * T_1(t) + [L_2(\omega)] * T_2(t) + [NR(\omega)] * T_3(t)$$
 eq. 2

Each T_n represents the different dynamics in question, which may contain molecular responses, denoted L_n , a nonresonant response, denoted NR, or a combination of both. The molecular resonances, L_n , are represented by Lorentzian lineshape functions, and the NR response is modeled by a constant. In this model, we associate both L_1 and NR with dynamics T_1 , only L_2 with dynamics T_2 , and only NR with dynamics T_3 . (Detailed model parameters are included in the supplementary materials S1). The goal was to test whether our

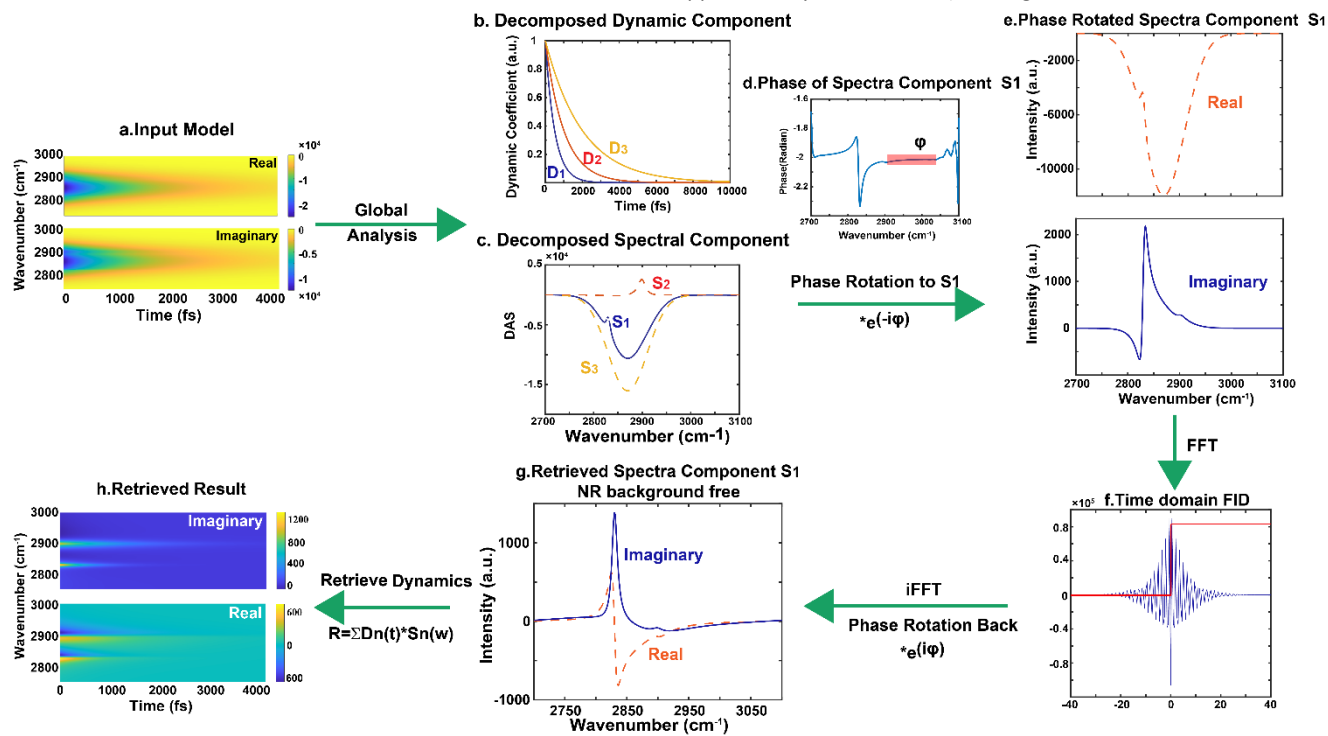


Figure 1. Flow chart of the data analysis method. The (a) initial input data was decomposed by global analysis (Glotaran) into various (b) dynamics and (c) spectral components. By inspecting the spectral components, S_1 contained a broad background which is the NR signal, and a small dip corresponding to a molecular feature, S_2 only had a sharp molecular feature and S_3 was only NR signal. Thus, we only needed to process S_1 to separate the molecular features from NR signals. We then determined the phase ϕ of NR signal from (d) the phase plot of S_1 . The flat phase region represented the NR phase, which should be a constant. By applying a phase rotation, (e) the NR signal was fully rotated to the real part of the phase rotated S_1 , whereas the imaginary part was composed of a molecular resonance. Then, we Fourier transformed only the imaginary spectra to get (f) the time domain free induction decay (FID) and applied a Heaviside function (red in f) to impose causality. The FID after causality was inverse Fourier transformed back and applied an inverse phase rotation to restore the original spectral phase. (g) The retrieved S_1 now was free of NR signal and only composed of molecular responses. The retrieved molecular dynamics, free from NR dynamics, could be composed of three spectral and dynamical components by equation: $R = \sum D_n(t) \otimes S_n(\omega)$, where \otimes is the outer products of vectors and D_n and S_n are the dynamical and spectral components n, after NR removal.

Journal Name COMMUNICATION

method could successfully extract different dynamics and their corresponding spectral components, and then further retrieve the molecular response components and reconstruct the hidden molecular dynamics. Therefore, the purpose of the model is solely to test the method and is not simulating or mimicking the experimental data we discussed later.

Before examining the fidelity of this method, we first introduce the full workflow of this data retrieval method (Fig.1, more detailed explanation and example code are included in supplementary materials Section 1). The constructed model input contains real and imaginary parts, and both appear as broad spectral dynamics that decay over a few picoseconds (Fig.1a). The broad spectra are due to the NR signal, which overwhelms the underlying molecular dynamics. The goal of the data analysis method is to retrieve the molecular dynamics by removing the one of the NR signals. First, we performed global analysis on the model input, using Glotaran³⁹, to decompose the dynamics into separate spectral and dynamic components. We found three distinct dynamics (Fig.1b), associated with three spectral components (Fig.1c). The number of distinct dynamics was consistent with the model input from Eq.2. Among all three spectral components, the spectrum of component 1 (S₁ in Fig.1c, solid blue) showed two features, whereas others had only single features: component 2 (S2 in Fig.1c, dashed red) showed a sharp Lorentzianshape feature, suggesting it is a pure molecular response, whereas component 3 (S₃ in Fig.1c, dashed yellow) was a broad Gaussian, indicating it is NR signal only. Thus, only S₁ was a mixture of both NR and molecular resonant features, which we needed to apply algorithms to extract the molecular feature from S₁.

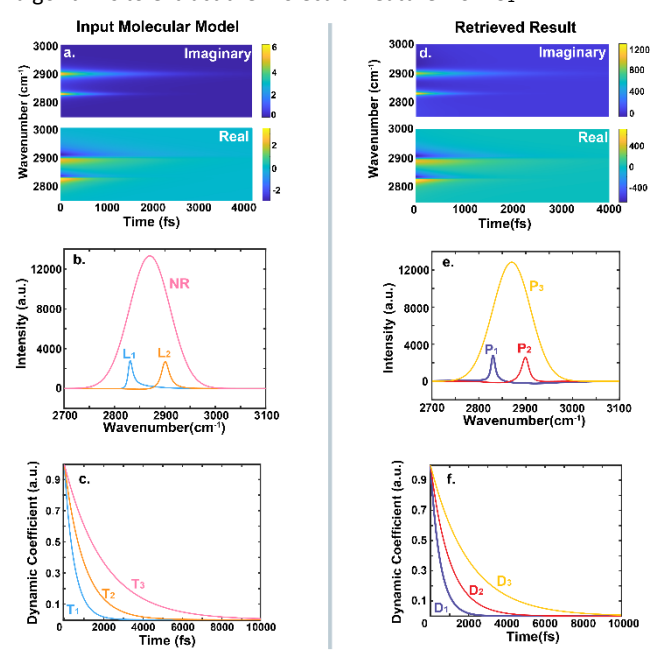


Figure 2. Comparison of (a-c) model input and (d-f) retrieved results. The full dynamics of model input is plotted in Fig 1.a, which was composed according to equation 2, by three spectral components and three dynamic components. After retrieval described in Fig.1, the retrieved (e) spectral and (f) dynamic components matched well with the initial input (b) and (c). Finally, based on the relationships between P and D, we could (d) reconstruct molecular dynamics, which extracted (a) the molecular dynamics of model input from the overall dynamics of the model (Fig.1a) well.

To remove the NR signal from S₁, we first determined the NR phase. As the NR signal's phase should be frequency-independent, we identified the NR phase (φ) from the flat region of the phase plot of S_1 (Fig.1d). Then, we multiplied $e^{-i\varphi}$ to the complex spectra of S_1 . This operation led to a new imaginary spectrum that only contained molecular resonant signals (solid blue in Fig.1e). We then applied Fourier-transform only to the new imaginary spectrum and transformed it into the time domain. We multiplied the time-domain dynamics by a Heaviside function to set time-domain responses in the negative time regime to be zero, the so-called causality (Fig.1f). After applying causality, the time-domain response was inversely Fourier transformed back and then multiplied by $e^{i \varphi}$ to restore their initial phase. These operations restored the real part of spectra (dashed red in Fig.1g), free from NR. Thus, we retrieved a full complex molecular response of S₁ (Fig.1g). Lastly, we could combine all three components to reconstruct the molecular dynamics, free from NR signal dynamics (Fig.1h). Comparing to the initial input (Fig.1a), the molecular dynamics had sharp spectral features.

Next, we examined the fidelity of this method by comparing the retrieved molecular spectra and dynamic components with the model input: the retrieved results highly resembled the initial input (Fig.2). First of all, the retrieved dynamics (Fig.2f were the same as the original input (Fig.2c): D_1 , D_2 , and D_3 could be assigned to T_1 , T_2 , and T_3 , respectively. This agreement is not surprising, as global analysis is established to identify distinguishable dynamics. Second, we retrieved all three spectral components with correct spectral positions, phase, and lineshape, with P_1 , P_2 , and P_3 corresponding to L_1 , L_2 , and NR, respectively. Third, the retrieved relationships between spectral and dynamic components matched with the initial input. From Fig.1b and c, we know that P_1 is from S_1 , and exhibits

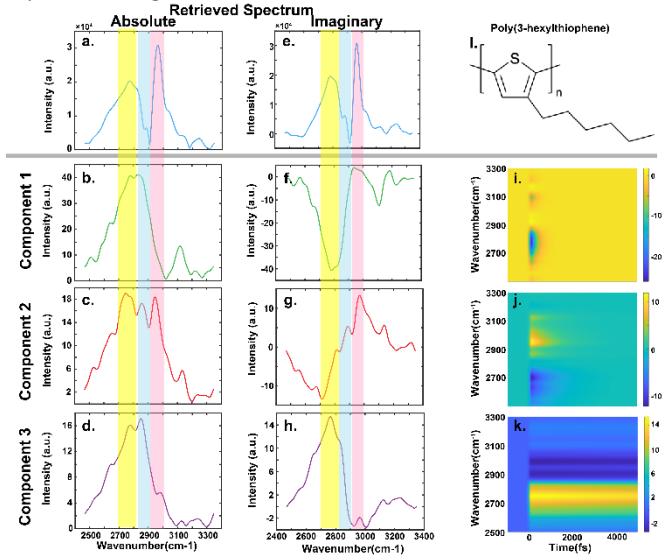


Figure 3. Retrieved spectral and dynamical components from an experimental transient VSFG scan on P3HT/Au interfaces. (a) The absolute static HD VSFG spectra of P3HT on Au had three major peaks, corresponding to electronic resonance (yellow), CH₂ FR (blue) and CH₃ AS (red). The transient spectral dynamics were decomposed into three components, including (i) coherent artifacts, (j) charge recombination and (k) charge separation. (b-d) The corresponding absolute spectral components showed the molecular peaks involved in each dynamic. A comparison between (e) the imaginary static VSFG spectra and (f-h) the imaginary parts of three transient spectral components shows the changes of spectral phase. (l) molecular structure of P3HT

COMMUNICATION Journal Name

dynamic T_1 . Similarly, P_2 shows the dynamics of T_2 , and P_3 has both T_1 and T_3 dynamics. These relationships matched with Eq.2. Lastly, the reconstructed molecular dynamics agree well with the molecular dynamics of original input (constructed based on Eq.2, without NR spectral components), demonstrating that this method could effectively remove significant NR dynamics and has the high fidelity required to restore underlying molecular dynamics from the original data.

Having validated this method, we applied it to the ultrafast dynamics of photo-induced direct charge transfer from gold to the organic semiconductor regioregular poly(3-hexylthiophene-2,5-diyl) or P3HT (Fig.3I). We collected this data using transient heterodyne VSFG spectroscopy, in which we used a near-IR 800 nm pulse to excite the interfaces and used HD VSFG signal to probe the transient responses at interfaces, upon charge transfer (please refer to Ref 22 for experimental details). The IR spectra were centered near 2900 cm⁻¹ to probe the various CH vibrational features. However, the thiophene ring mode can also be a probe feature to reveal the local electron dynamics. We showed that transient VSFG spectroscopy was sensitive to charge transfer dynamics due to the electric fieldinduced effects, firstly demonstrated in the SHG.⁴⁰ The electric fieldinduced effect is a third-order nonlinear signal, which is induced by the additional static electric field at interfaces acting on the sample, together with the VSFG pulse sequences, e.g., $\chi^{(3)}E_{interface}$. ^{33–38} This new signal is, therefore, proportional to the interfacial static fields. When charge transfer occurs at interfaces, the free charge carriers can generate electric fields across interfaces, triggering the electric field-induced VSFG signal.¹⁹ The new signal appears as a transient, which is used to track charge dynamics. In our previous work, the mechanistic study showed that for specific molecular conformations, a new interfacial bandgap was formed between Fermi Level of gold and conduction band of P3HT, which allowed the near-IR pulse to promote electrons from the metal to the organic semiconductors directly.18

The spectral dynamics also showed molecular responses, but it was overwhelmed by the dominating dynamics of the NR background. We had not been able to separate the underline molecular dynamics in our previous work fully. We here extract molecular dynamics from the raw scan (Fig.4a and b). The retrieved results are shown in Fig.3. We identified three distinct dynamics, consistent with previous results.²² Component 1 decayed in 264 fs (Fig.3i), which was a nonlinear response due to overlap of laser pulses, known as the coherent artifact. The coherent artifact does not reflect molecular dynamics. Component 2 decayed in 940 fs (Fig.3j), which corresponded to excited excitons quickly recombining with each other; component 3 had a long lifetime and was attributed to separated free charges (Fig.3k).

The extracted spectral components in Fig.3 reveal more details about the molecular dynamics. We compared the absolute spectra (Fig.3b-d) with the static absolute VSFG spectra (Fig.3a) of the P3HT on gold, in which the NR signal had been removed using the same method. In the static spectra, we could identify three significant peaks at 2953

cm⁻¹, 2875 cm⁻¹, and 2774 cm⁻¹, corresponding to CH₃ asymmetric stretch (AS, pink bar in Fig.3a-d), CH₂ Fermi resonance (FR, blue bar) and an electronic mode (yellow bar). 18 The electronic mode is likely to be an interfacial electronic state, which is resonant with the sum of the IR and up-conversion frequency, e.g., 2774 cm⁻¹+ 12500 cm⁻¹ (or 654 nm), generating an electronic SFG signal. 41 We note that the electronic feature is narrow, likely due to that our spectral coverage only captured the blue tail of the electronic resonance. By comparing it with the three transient spectral components, we identified molecular resonances involved in each dynamic. The electronic modes dominated all three components because electronic resonances had much larger dipole than molecular modes. Also, the CH₃ AS and CH₂ FR modes were present in the electron recombination dynamics, and show small responses in the separation dynamics. The significant amplitudes of CH₃ AS and CH₂ FR modes in the electron recombination dynamics (component 2) suggests that the excited excitons that underwent recombination, localized near the P3HT side chains, and led to a large perturbation to the hydrocarbon modes. This result suggested excitons near hydrocarbon chains of P3HT are prone to charge recombination.

Next, we inspected the retrieved imaginary spectra to learn the phase changes of molecular responses during charge dynamics. The charge recombination dynamics led to a large negative peak for the electronic resonance, which is a population bleach, suggesting the charges occupied this electronic state before recombination. For charge separation dynamics, the electronic resonance in the transient spectra had the same phase as in the static spectra. Because this transient spectral feature was induced by local electric fields of free charges, its phase indicated that the charge-induced electric fields and this interfacial electronic dipole pointed in the same direction. The electronic dipoles that have the same direction as the induced electric field could promote charge separation dynamics, by repelling the electron-hole pairs away from interfaces. This relative orientation between dipoles and the transient electric fields could provide critical insights into the molecular dipole's role

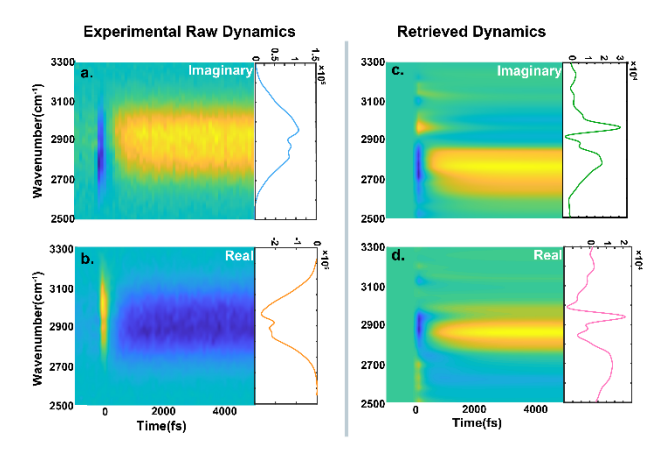


Figure 4. A comparison between imaginary and real parts of (a and b) experimental raw dynamics of charge transfer at P3HT/Au interfaces (and corresponding linear VSFG spectra, right), and (c and d) retrieved molecular dynamics (and corresponding molecular contribution to the liner VSFG spectra, right). The retrieved results (c and d) show the dynamics of three molecular resonance of P3HT, which is overwhelmed by the dynamics of large NR background in a and b.

Journal Name COMMUNICATION

in interfacial charge transfer dynamics. It also warrants further high-level simulation studies to fully corroborate the role of molecules in charge transfer dynamics at the atomic level. 42

We lastly compared the fully reconstructed molecular dynamics of interfacial charge transfer (Fig. 4c and d) with the original experimental input (Fig.4a and b). The molecular electronic response near 2770 cm⁻¹ dominated the extracted dynamics, with a small contribution from P3HT's CH₂ and CH₃ vibrations. This molecular electronic dynamic was hidden in the original data by the large NR dynamics (Fig.4a and b). We found the retrieved molecular electronic state dynamics exhibit a fast-decaying negative dynamic, followed by a positive, long-lived dynamic, corresponding to the long-lifetime separated free charges. The extracted molecular dynamics were similar to the NR signal, which suggested that P3HT molecules participated in all charge dynamics at the interfaces.

Conclusions

We showed that by applying a new data retrieval method to the transient heterodyne VSFG spectral scans, we could extract time-dependent molecular responses from charge dynamics induced by photoexcitation in complex materials. In this example, we found that the organic P3HT molecules were involved in all charge dynamics at interfaces, and the direction of the electronic dipole and electric fields at interfaces suggested that the dipole could help charge separation by repulsion. In the future, this method will be useful to dissect dynamics of interfaces composed of multiple molecular species into specific molecular dynamics, thereby revealing hidden dynamics of different molecules at interfaces of heterojunction systems, such as photoelectrical catalysis, molecular quantum heterojunctions, and optoelectronic materials.

Conflicts of interest

There are no conflicts to declare.

Notes and references

- W. A. Tisdale, K. J. Williams, B. A. Timp, D. J. Norris, E. S.
 Aydil and X. Y. Zhu, Science (80-.)., 2010, 328, 1543–1547.
- 2 R. D. Pensack and J. B. Asbury, *J. Phys. Chem. Lett.*, 2010, 1, 2255–2263.
- 3 G. Grancini, M. Biasiucci, R. Mastria, F. Scotognella, F. Tassone, D. Polli, G. Gigli and G. Lanzani, *J. Phys. Chem. Lett.*, 2012, **3**, 517–523.
- 4 A. E. Jailaubekov, A. P. Willard, J. R. Tritsch, W. L. Chan, N. Sai, R. Gearba, L. G. Kaake, K. J. Williams, K. Leung, P. J. Rossky and X. Y. Zhu, *Nat. Mater.*, 2013, **12**, 66–73.
- 5 K. Wu, J. Chen, J. R. McBride and T. Lian, *Science (80-.).*, 2015, **349**, 632–635.
- 6 W. Xiong, J. E. Laaser, P. Paoprasert, R. A. Franking, R. J. Hamers, P. Gopalan and M. T. Zanni, *J. Am. Chem. Soc.*, 2009, **131**, 18040.

- 7 H. Zhu, J. Wang, Z. Gong, Y. D. Kim, J. Hone and X. Y. Zhu, Nano Lett., 2017, 17, 3591.
- W. H. Hung, K. L. Yang, S. N. Lai, C. R. Yang, J. J. Shyue, C. S. Ku and S. B. Cronin, *J. Mater. Chem. A*, 2017, 5, 10687–10695.
- 9 M. Scarongella, A. Laktionov, U. Rothlisberger and N. Banerji, *J. Mater. Chem. C*, 2013, **1**, 2308–2319.
- 10 Q. Zhang, X. Liu, F. Jiao, S. Braun, M. J. Jafari, X. Crispin, T. Ederth and M. Fahlman, *J. Mater. Chem. C*, 2017, **5**, 275–281.
- 11 H. Zhu, J. Wang, Z. Gong, Y. D. Kim, J. Hone and X. Y. Zhu, *Nano Lett.*, 2017, **17**, 3591–3598.
- 12 X. Zhu, N. R. Monahan, Z. Gong, H. Zhu, K. W. Williams and C. A. Nelson, *J. Am. Chem. Soc.*, 2015, 137, 8313–8320.
- 13 Y. Fu, H. Zhu, J. Chen, M. P. Hautzinger, X. Y. Zhu and S. Jin, *Nat. Rev. Mater.*, 2019, 4, 169–188.
- Y. Garcia-Basabe, G. G. Parra, M. B. Barioni, C. D. Mendoza, F. C. Vicentin and D. Larrudé, *Phys. Chem. Chem. Phys.*, 2019, **21**, 23521–23532.
- P. Dhar, P. P. Khlyabich, B. Burkhart, S. T. Roberts, S. Malyk,
 B. C. Thompson and A. V. Benderskii, J. Phys. Chem. C,
 2013, 117, 15213–15220.
- 16 H. T. Yi, X. Wu, X. Zhu and V. Podzorov, *Adv. Mater.*, 2016, 28, 6509–6514.
- G. H. Deng, Y. Qian, Q. Wei, T. Zhang and Y. Rao, J. Phys. Chem. Lett., 2020, 11, 1738–1745.
- B. Xiang, Y. Li, C. H. Pham, F. Paesani and W. Xiong, *Sci. Adv.*, 2017, 3, e1701508.
- T. C. Anglin, D. B. O'Brien and A. M. Massari, *J. Phys. Chem. C*, 2010, **114**, 17629–17637.
- 20 I. Yagi, K. Inokuma, K. Kimijima and H. Notsu, *J. Phys. Chem. C*, 2014, **118**, 26182–26190.
- Y. C. Wen, S. Zha, X. Liu, S. Yang, P. Guo, G. Shi, H. Fang, Y.R. Shen and C. Tian, *Phys. Rev. Lett.*, 2016, **116**, 016101.
- Y. Li, B. Xiang and W. Xiong, J. Chem. Phys., 2019, 150, 114706.
- 23 G. Neri, J. J. Walsh, G. Teobaldi, P. M. Donaldson and A. J. Cowan, *Nat. Catal.*, 2018, **1**, 952–959.
- 24 P. C. Singh, S. Nihonyanagi, S. Yamaguchi and T. Tahara, J. Chem. Phys., 2012, 137, 094706.
- 25 S. Nihonyanagi, P. C. Singh, S. Yamaguchi and T. Tahara, *Bull. Chem. Soc. Jpn.*, 2012, **85**, 758–760.
- 26 W. C. Yang and D. K. Hore, J. Phys. Chem. C, 2017, 121, 28043–28050.
- 27 H. Vanselous and P. B. Petersen, J. Phys. Chem. C, 2016, 120, 8175–8184.
- I. V. Stiopkin, H. D. Jayathilake, A. N. Bordenyuk and A. V. Benderskii, *J. Am. Chem. Soc.*, 2008, **130**, 2271–2275.
- 29 B. Xu, Y. Wu, D. Sun, H.-L. Dai and Y. Rao, *Opt. Lett.*, 2015, **40**, 4472.
- 30 H. Wang, T. Gao and W. Xiong, *ACS Photonics*, 2017, **4**, 1839–1845.
- 31 W. Hua, X. Chen and H. C. Allen, *J. Phys. Chem. A*, 2011, **115**, 6233–6238.
- 32 Y. Han, V. Raghunathan, R. R. Feng, H. Maekawa, C. Y. Chung, Y. Feng, E. O. Potma and N. H. Ge, *J. Phys. Chem. B*, 2013, **117**, 6149–6156.

COMMUNICATION Journal Name

- A. M. Darlington, T. A. Jarisz, E. L. Dewalt-Kerian, S. Roy, S. Kim, M. S. Azam, D. K. Hore and J. M. Gibbs, *J. Phys. Chem. C*, 2017, **121**, 20229–20241.
- P. E. Ohno, H. F. Wang, F. Paesani, J. L. Skinner and F. M. Geiger, *J. Phys. Chem. A*, 2018, **122**, 4457–4464.
- 35 M. Doğangün, P. E. Ohno, D. Liang, A. C. McGeachy, A. G. Bé, N. Dalchand, T. Li, Q. Cui and F. M. Geiger, *J. Phys. Chem. B*, 2018, **122**, 4870–4879.
- 36 S. K. Reddy, R. Thiraux, B. A. Wellen Rudd, L. Lin, T. Adel, T. Joutsuka, F. M. Geiger, H. C. Allen, A. Morita and F. Paesani, *Chem*, 2018, **4**, 1629–1644.
- 37 S. Roy, C. Beutier and D. K. Hore, *J. Mol. Struct.*, 2018, **1161**, 403–411.
- S. Pezzotti, D. R. Galimberti, Y. R. Shen and M. P. Gaigeot,
 Phys. Chem. Chem. Phys., 2018, 20, 5190–5199.
- J. J. Snellenburg, S. Laptenok, R. Seger, K. M. Mullen and I.H. M. van Stokkum, J. Stat. Softw., 2012, 49, 1–22.
- 40 C. H. Lee, R. K. Chang and N. Bloembergen, *Phys. Rev. Lett.*, 1967, **18**, 167–170.
- 41 Y. Li, J. Wang and W. Xiong, *J. Phys. Chem. C*, 2015, **119**, 28083–28089.
- 42 V. O. Özçelik, Y. Li, W. Xiong and F. Paesani, *J. Phys. Chem. C*, 2020, **124**, 4802–4809.